Bulletin of the Seismological Society of America, Vol. 86, No. 1A, pp. 212–220, February 1996

The Accuracy of Seismic Estimates of Dynamic Strains: An Evaluation Using Strainmeter and Seismometer Data from Piñon Flat Observatory, California

by Joan Gomberg and Duncan Agnew

Abstract The dynamic strains associated with seismic waves may play a significant role in earthquake triggering, hydrological and magmatic changes, earthquake damage, and ground failure. We determine how accurately dynamic strains may be estimated from seismometer data and elastic-wave theory by comparing such estimated strains with strains measured on a three-component long-base strainmeter system at Piñon Flat, California. We quantify the uncertainties and errors through cross-spectral analysis of data from three regional earthquakes (the $M_0 = 4 \times 10^{17}$ N-m St. George, Utah; $M_0 = 4 \times 10^{17}$ N-m Little Skull Mountain, Nevada; and $M_0 = 1 \times 10^{19}$ N-m Northridge, California, events at distances of 470, 345, and 206 km, respectively). Our analysis indicates that in most cases the phase of the estimated strain matches that of the observed strain quite well (to within the uncertainties, which are about ± 0.1 to ± 0.2 cycles). However, the amplitudes are often systematically off, at levels exceeding the uncertainties (about 20%); in one case, the predicted strain amplitudes are nearly twice those observed. We also observe significant $\varepsilon_{\phi\phi}$ strains (ϕ = tangential direction), which should be zero theoretically; in the worst case, the rms $\varepsilon_{\phi\phi}$ strain exceeds the other nonzero components. These nonzero $\varepsilon_{\phi\phi}$ strains cannot be caused by deviations of the surface-wave propagation paths from the expected azimuth or by departures from the plane-wave approximation. We believe that distortion of the strain field by topography or material heterogeneities give rise to these complexities.

Introduction

The dynamic strains caused by the passage of seismic waves play a significant role in a number of physical processes. In some cases, very small differences in the characteristics of the dynamic strain field may make considerable differences in the processes they initiate. Since there are relatively few direct measurements of strains (compared to the large number of seismic measurements), it is therefore important to determine how well we can estimate the strain field, either from available seismic data or from theoretical computations. We attempt to do this by comparing three-component seismic and strain data from three regional earthquakes. The frequency content of these data may be relevant to earthquake triggering and is of engineering significance for tall or spatially extended structures. The results should scale linearly to smaller and larger strain amplitudes, until extremely large strains occur causing nonlinear responses such as ground failure.

Dynamic strains associated with the surface waves generated by the M_S 7.4 Landers earthquake have been identified as causing, or at least initiating, seismicity increases at regional and remote distances (Hill *et al.*, 1993; Anderson *et al.*, 1994; Gomberg and Bodin, 1994; Linde *et al.*, 1994; Gomberg, 1996). Data and theoretical estimates of the dynamic strains from the Landers and other earthquakes suggest that there is a relatively sharp triggering threshold. Dynamic strain amplitudes associated with the Landers earthquake varied by less than a factor of 2 between sites where triggered seismicity did and did not occur (Hill *et al.*, 1993; Anderson *et al.*, 1994; Gomberg, 1996). Further refinement of these apparent triggering thresholds should provide an important constraint on the triggering mechanisms. However, this will require estimates of the complete strain field as well as knowledge of their accuracy.

The ability to estimate dynamic strains accurately also has significant engineering implications. Dynamic strains associated with seismic surface waves probably cause earthquake damage at distances of tens to hundreds of km. Seismograph array data for aftershocks of the Northridge earthquake show significant differential ground displacements (i.e., strains) at points separated by ~100 to 300 m

(Spudich *et al.,* 1994; Meremonte *et al.,* 1994; Cranswick *et al.,* 1994). The extent to which different motions are applied to spatially separated parts of the base of an extended structure is an important engineering consideration (Jeng and Kasai, 1994; Der Kiureghian, 1994; Zerva, 1992a). Dynamic strains have also been implicated in certain types of ground failure such as liquefaction (Seed and Idriss, 1971; Drnevich and Richart, 1970; Dobry *et al.,* 1981; O'Rourke and Castro, 1981; Holzer *et al.,* 1989; Mavko and Harp, 1984; Stewart and Hussein, 1992) and in the failure of buried structures such as pipelines (Ariman and Hamada, 1981; O'Rourke and Castro, 1981; Nisho, 1989; Zerva, 1992b).

We compare direct estimates of dynamic strains measured by strainmeters with more approximate estimates made from data recorded by inertial seismometers. The fact that these instruments record different quantities and that combining recordings from them would provide information available from neither considered in isolation is not a new idea. This idea and some of the basic equations are contained in the article of Benioff (1935), in which he described the first successful strain seismograph. This article, and a later one by Benioff and Gutenberg (1952), focused on the difference in azimuthal response (for different types of seismic waves) between linear extension and ground displacement. They proposed to combine records to determine which type of wave motion was associated with particular phases. Romney (1964) further developed this by proposing to use the different responses of strainmeters and seismometers to discriminate between noise and *P* waves. This inspired a substantial research effort (summarized by Fix, 1973) into combined strainmeter and seismograph installations, though apparently few were very successful. A novel reason for combining strain and displacement records was given by Mikumo and Aki (1964). They pointed out that since the ratio of strain to displacement depended on phase velocity, one could combine strain and displacement records to estimate phase velocity, rather than using an array of stations. Mikumo and Aki were restricted by the data available to a single component of strain and horizontal displacement, using instruments that lacked adequate calibration. Sacks *et al.* (1976) pointed out some of the difficulties in using this technique at very long periods (>100 sec) because of the effect of tilt on horizontal inertial instruments. They suggested using dilational strain and vertical motion data instead, at least for those wave types for which these are not zero. They did not, however, examine any data. Borcherdt *et al.* (1988) examined ground-motion and strain data for *P* and *S* waves from several local and regional earthquakes and found fair agreement with the theory developed by Borcherdt (1989), though this theory and the data were restricted to a single component of strain (dilatation).

Data

Except for this last article, all of the above studies essentially assumed that simple plane-wave propagation theory was an accurate predictor of the relation between strains and displacements (and their time derivatives). Our purpose here is to test the accuracy of this predictor, especially for surface waves, which account for the peak strains from regional earthquakes. We require accurate measurements of all three components of strain at seismic frequencies. Unfortunately, few such measurements are available. A large amount of earthquake data have been collected using Sacks-Evertson dilatometers (Agnew 1986), but these only record a scalar combination of vertical and areal strain. Of the many mechanical extensometers now in operation, most are not set up to record at the frequencies of interest, many are not adequately calibrated (Beaumont and Berger, 1975), and all are housed in natural or artificial cavities that distort the strain field in unpredictable ways. Although it is in principle possible to remove this effect through calibration with the earth tides, this has not been done with much success (Emter and Zurn, 1983).

We have therefore used data from the only site at which the surface strain tensor is measured, at Piñon Flat Observatory (PFO) in California (Fig. 1). The PFO strainmeter consists of three 732-m laser interferometers (Berger and Lovberg, 1970). These have resolution of about 10^{-4} μstrain at seismic frequencies, sufficient to resolve ground noise for frequencies from 0.05 to 1 Hz. Since the basis of the system is counting interference fringes, the calibration is known to 0.1% (the uncertainty arising from the uncertainty in the base length), and the system is completely linear up to the limit of the fringe-counting system (± 3.2 μstrain), though the recording system used here has an upper limit of ± 0.2

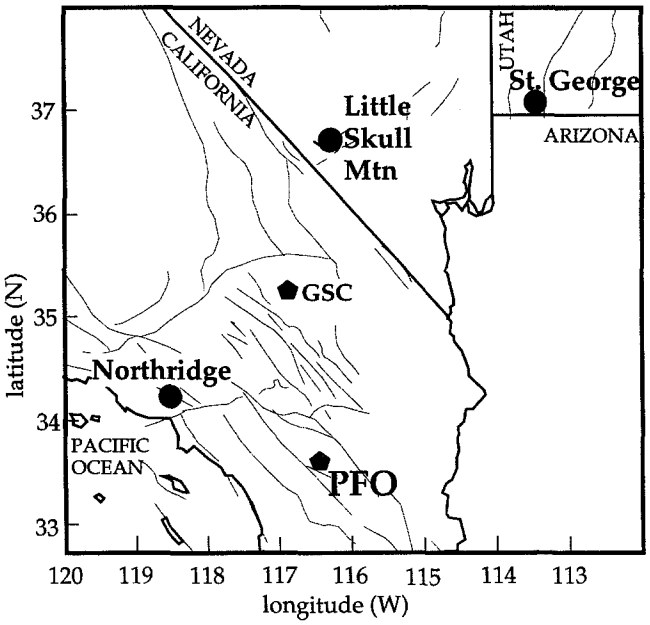

Figure 1. Map showing the locations of the Piñon Flat Observatory (PFO) and TERRAscope station GSC (pentagons) and epicenters (black dots) of the three earthquakes studied (Table 1). Thin lines are mapped fault traces.

μstrain. (While accelerations over 0.1 g have caused loss of fringe lock, this exceeds the accelerations from the regional events we discuss by several orders of magnitude.) The response of the counting system is flat for frequencies from 0 Hz to 1 MHz, but because the baselength of the system causes spatial aliasing for frequencies above 10 Hz, the output recorded is filtered with a 4-pole analog low-pass filter with poles at 2 Hz. This yields an amplitude response that for frequencies below ~0.5 Hz is essentially flat in amplitude and has a nearly constant phase delay of -0.3 seconds. The data are recorded at 10 Hz, so there is no significant aliasing.

Several seismometers are operated at PFO; the data we use come from a Streckeisen STS-1 system that is operated by the IDA/IRIS group and also recorded as part of the TERRAscope project (Kanamori *et al.*, 1991). For frequencies from 0.003 to 0.5 Hz, the data recorded (at 20 Hz) are essentially equivalent to ground velocity. The noise in the system is set by local ground noise (IRIS, 1994), which is at least two orders of magnitude below the levels of the signals presented here.

Estimation of Surface Dynamic Strains from Ground Velocity Recordings

For shallow earthquakes, the dominant energy in the seismic wave field at distances of several tens to hundreds of kilometers is in surface waves with periods of several to tens of seconds. At these distances, body-wave phases may be synthesized by summing a sufficient number of surface-wave modes. We summarize the theory behind strain estimation from seismograms recorded at these distances to elucidate the potential errors attributable to the underlying approximations. The first fundamental assumption made is that the seismic energy travels as plane waves. The second assumption is that the medium is laterally homogenous or that the scale of any lateral variation in material properties exceeds the wavelengths of the dominant energy (ranging from ~5 to 150 km for periods of ~2 to 40 sec). In the latter case, in which the heterogeneity is "slowly varying," the deformation at a point may be treated as if the medium is locally homogeneous (Woodhouse, 1974).

We first derive expressions relating dynamic strains to quantities measurable from seismograms. For laterally homogeneous media at regional distances, the solutions to the elastic wave equation are most appropriately derived by expressing the displacement field as an expansion of cylindrical harmonics,

$$Y = J_m(kr)e^{im\phi}, \tag{1}$$

where $J_m(kr)$ is a Bessel function of order m, k is the wavenumber, r is the receiver-source distance, and ϕ is the receiver-source azimuth. The nonzero surface strains are

$$\varepsilon_{rr} = \frac{B(z)}{k}\frac{\partial^2 Y}{\partial r^2} + \frac{imC(z)}{kr}\left(\frac{\partial Y}{\partial r} - \frac{Y}{r}\right) \quad \varepsilon_{zz} = Y\frac{\partial A(z)}{\partial z}$$

$$\varepsilon_{\phi\phi} = \frac{B(z)}{kr}\left(\frac{\partial Y}{\partial r} - m^2\frac{Y}{r}\right) - \frac{imC(z)}{kr}\left(\frac{\partial Y}{\partial r} - \frac{Y}{r}\right)$$

$$\varepsilon_{r\phi} = \frac{1}{2}\left[\frac{2imB(z)}{kr}\left(\frac{\partial Y}{\partial r} - \frac{Y}{r}\right) + \frac{C(z)}{kr}\left(\frac{\partial Y}{\partial r} - m^2\frac{Y}{r} - r\frac{\partial^2 Y}{\partial r^2}\right)\right]. \tag{2}$$

The mode numbers have been omitted from the vertical eigenfunctions, $A_n(z)$, $B_n(z)$, and $C_n(z)$ and the wavenumber, k_n, for clarity. The radial, tangential, and vertical displacements, u_r, u_ϕ, and u_z, respectively, are

$$u_r\hat{r} = \left(\frac{B(z)}{k}\frac{\partial Y}{\partial r} + \frac{imC(z)}{k}\frac{Y}{r}\right)\hat{r}$$

$$u_\phi\hat{\phi} = \left(\frac{imB(z)}{k}\frac{Y}{r} - \frac{C(z)}{k}\frac{\partial Y}{\partial r}\right)\hat{\phi}$$

$$u_z\hat{z} = A(z)Y\hat{z}. \tag{3}$$

These expressions may be simplified at large r by neglecting terms decaying as Y/r, and writing the strains in terms of the displacements as

$$\varepsilon_{rr} = \frac{\partial\tilde{\mu}_r}{\partial r} - im\frac{\tilde{\mu}_\phi}{r} \quad \varepsilon_{zz} = \frac{\partial u_z}{\partial z}$$

$$\varepsilon_{\phi\phi} = \frac{\tilde{\mu}_r}{r} + im\frac{\tilde{\mu}_\phi}{r}$$

$$\varepsilon_{r\phi} = \frac{1}{2}\left[2im\frac{\tilde{\mu}_r}{r} - \frac{\tilde{u}_\phi}{r} + \frac{\partial\tilde{\mu}_\phi}{\partial r}\right], \tag{4}$$

where $\tilde{\mu}_r$ and $\tilde{\mu}_\phi$ are the simplified, approximate displacements. If we then neglect the terms equivalent to the curvature of the cylindrical wavefronts, $\sim\tilde{\mu}_r/r$ and $\sim\tilde{\mu}_\phi/r$, approximating them as plane waves, the approximate strains result. These are (for a single mode)

$$\hat{\varepsilon}_{rr} \approx \frac{\partial\tilde{\mu}_r}{\partial r} = -\frac{1}{\hat{C}_R}\frac{\partial\tilde{\mu}_r}{\partial t} \quad \varepsilon_{zz} = \frac{\partial u_z}{\partial z}$$

$$\varepsilon_{\phi\phi} \approx 0$$

$$\varepsilon_{r\phi} \approx \frac{1}{2}\frac{\partial\tilde{\mu}_\phi}{\partial r} = -\frac{1}{2C_L}\frac{\partial\tilde{\mu}_\phi}{\partial t}. \tag{5}$$

The right-most terms of the ε_{rr} and $\varepsilon_{r\phi}$ strains derive from approximating the Bessel function as a Hankel function (equation 1), which is appropriate at large values of kr. C_R and C_L are the Rayleigh and Love phase velocities, respec-

tively, and t is time. Equations (4) and (5) show that the ε_{rr} and $\varepsilon_{r\phi}$ strains may be estimated directly from radial and tangential seismograms and knowledge of the phase velocities appropriate to the particular structure at the place of observation. The equations also show that the $\varepsilon_{\phi\phi}$ strain should be zero and that the ε_{zz} strain cannot be estimated from surface seismic data (which measure only u_z, not its derivative with depth).

Horizontal-component seismograms of the Northridge, Little Skull Mountain, and St. George earthquakes (Table 1) were analyzed to obtain ε_{rr} and $\varepsilon_{r\phi}$ strain estimates. The processing steps were (1) correct the seismic data for the seismometer response to produce ground-velocity records; (2) rotate horizontal components to calculated radial and tangential directions; (3) low-pass filter the data (using a Butterworth filter with 24 db/octave roll-off above a corner frequency of 1 Hz) and decimate to 10 Hz (to match the strain data); (4) Fourier transform the data and divide the spectra by calculated fundamental mode phase velocities (to produce strain spectra); and finally, (5) inverse Fourier transform to get an estimated strain time series. Assuming only a single mode will not introduce a significant error if the strains are dominated by the fundamental mode or if the higher-mode phase velocities are not significantly different.

Estimation of Surface Dynamic Strains from Recordings of Linear Strains

We next summarize the steps involved in deriving ε_{rr}, $\varepsilon_{r\phi}$, and $\varepsilon_{\phi\phi}$ strains from the PFO strainmeter data. The PFO strainmeters measure linear strains oriented very nearly north–south, east–west, and northwest–southeast. We define a global coordinate system as north $= +\hat{y}$, east $= +\hat{x}$, and up $= +\hat{z}$. The local coordinate system for each earthquake defined at PFO is also right-handed with up $= +\hat{z}$ and $+\hat{r}$ pointing radially away from the source. Extensional strains are negative. We consider the nonzero surface strain tensors components as vector $\boldsymbol{\varepsilon}^{\text{local}} = [\varepsilon_{rr}, \varepsilon_{\phi\phi}, \varepsilon_{r\phi}]^T$ and $\boldsymbol{\varepsilon}^{\text{global}} = [\varepsilon_{xx}\ \varepsilon_{yy}, \varepsilon_{xy}]^T$. After correction for the strainmeter response, and low-pass filtering to match the seismic data, the linear strains transform to $\boldsymbol{\varepsilon}^{\text{global}}$ using the definition of a linear strain:

$$\lambda = [\varepsilon_{xx}\cos^2\theta + \varepsilon_{yy}\sin^2\theta + 2\varepsilon_{xy}\cos\theta\sin\theta], \quad (6)$$

in which linear strain, λ, measures along an angle θ from $+\hat{x}$. $\boldsymbol{\varepsilon}^{\text{global}}$ is then rotated to $\boldsymbol{\varepsilon}^{\text{local}}$ using a rotation matrix,

$$\boldsymbol{\varepsilon}^{\text{global}} = \underline{R}\boldsymbol{\varepsilon}^{\text{local}}$$

$$\underline{R} = \begin{vmatrix} \sin^2\phi & \cos^2\phi & 2\sin\phi\cos\phi \\ \cos^2\phi & \sin^2\phi & -2\sin\phi\cos\phi \\ -\sin\phi\cos\phi & \sin\phi\cos\phi & \sin^2\phi - \cos^2\phi \end{vmatrix}, \quad (7)$$

where ϕ is the azimuth from receiver to source measured clockwise from the north. For two of the events, the relative timing could be checked through a cross-spectral analysis with a separate data stream (aliased for the events of interest here) and is good to 0.05 sec; for the Little Skull Mountain event, the strain data timing is uncertain to within 0.6 sec.

Figure 2 shows the ε_{rr}, $\varepsilon_{r\phi}$ strains derived from both the seismic and the strainmeter data. Although the theory predicts that the $\varepsilon_{\phi\phi}$ strains should be zero, the strainmeter results in Figure 2 clearly contradict this prediction. We explore the possible causes underlying this result in the final section.

How Accurate Are the Seismic Estimates of Strain?

Our approach to evaluating of the accuracy of strains estimated from seismic data assumes that the strainmeter signals are the true strains. Comparison of average or peak properties of the strainmeter and seismic strain estimates may result in overly pessimistic estimates of the probable errors; i.e., there may be certain frequency bands in which the strains can be predicted more accurately than indicated by a peak or average measures. Inferences often are drawn from the amplitude and/or the phase of the dynamic strain field. Therefore, we use a cross-spectral analysis technique that permits calculation of the uncertainties associated with both amplitude and phase estimates (Berger *et al.,* 1979). Prediction of the strainmeter data from the seismograms is posed as a filter estimation problem in which the slowness, $p = C^{-1}$, equals the filter. Note that equation (5) implies that, for a single mode or for multiple modes with phase velocities of similar functional forms, the true ε_{rr} and $\varepsilon_{r\phi}$ strains may be determined from velocity seismograms given knowledge of the correct phase velocities for each path at each frequency, f. The characteristics of the estimated slowness, or seismogram filter, and its uncertainties therefore provide a quantitative measure of the accuracy of the seismogram strain estimates.

Table 1
Horizontal-Component Seismogram Analyses for the Three Earthquakes Studied

Earthquake	Date	Moment (N-m)	Distance from PFO (km)	Azimuth from PFO (degrees from N)
Northridge, California	17 January 1994	1.2×10^{19}	206	290
Little Skull Mountain, Nevada	29 June 1992	4.1×10^{17}	345	2
St. George, Utah	2 September 1992	3.9×10^{17}	470	34

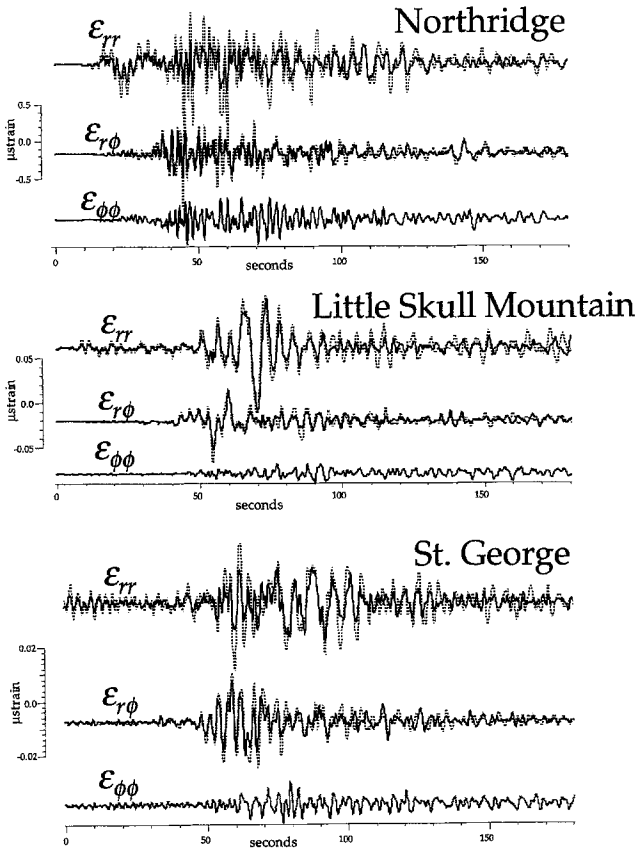

Figure 2. ε_{rr}, $\varepsilon_{r\phi}$ strains (upper, center traces) calculated from TERRAscope seismograms (dashed lines) and strainmeter data (sold lines). $\varepsilon_{\phi\phi}$ strains are only shown for the strainmeter data (lower traces) because the theory underlying the calculation of strains from the seismic data requires $\varepsilon_{\phi\phi} = 0$. Traces have been shifted to account for clock error; timing shifts are 0.6, 0.5, and -0.1 sec for the Northridge, Little Skull Mountain, and St. George data, respectively.

Following Berger *et al.* (1979), the approximate (denoted by the hat) seismic strain estimate, $\hat{\varepsilon}(f)_{rr}$, is

$$\hat{\varepsilon}(f)_{rr} = \hat{p}(f)_R \frac{\partial \tilde{u}(f)_r}{\partial t}, \tag{10}$$

and the strainmeter or true strain, $\varepsilon(f)_{rr}$, is

$$\varepsilon(f)_{rr} = p(f)_R \frac{\partial \tilde{u}(f)_r}{\partial t} \approx \hat{p}(f)_R \Delta p(f)_R \frac{\partial \tilde{u}(f)_r}{\partial t}; \tag{11}$$

$\Delta p(f)$ "corrects" the initial slowness or filter calculated from an Earth model. This correction is calculated according to

$$\Delta p(f) = \frac{\overline{\hat{\varepsilon}(f)_{rr}\varepsilon(f)^*_{rr}}}{\overline{\hat{\varepsilon}(f)_{rr}\hat{\varepsilon}(f)^*_{rr}}}. \tag{12}$$

The bars in equation (12) indicate smoothed spectral estimates, and the asterisk denotes the complex conjugate. Equivalent expressions may be written for the $r\phi$ component. Confidence intervals can also be calculated for the amplitude and phase of $\Delta p(f)$ (Jenkins and Watts, 1968). Because $C(f)$ is real, the phase of $\Delta p(f)$ should be zero. Moreover, $C(f)$ is a smooth function of f, and thus, $|\Delta p(f)|$ should also be smooth. We interpret deviations from these two characteristics as indicative of error in the underlying assumptions. We evaluate amplitude variability subjectively, guided by theoretical phase velocity curves calculated for a range of velocity/density structures.

Figure 3 shows the amplitude and phase estimates of $\Delta p(f)$ (equation 12), with calculated 95% confidence intervals for the three earthquakes recorded at PFO. Fundamental mode phase velocities, or slownesses, were calculated for a model of the velocity/density structure derived for a path between PFO and TERRAscope station GSC (Fig. 1; Wang and Teng, 1994). The phase estimates for the Little Skull Mountain and St. George earthquake data indicate that, at a given frequency, the true dynamic strain phase can be estimated within $\pm 10\%$ of a cycle below $\sim$0.15 Hz; at higher frequencies, uncertainties increase slightly, except in a few narrow bands where they rise to as much as $\pm 40\%$. The uncertainties of the Northridge estimates are somewhat higher. Only in a few frequency bands is the phase significantly different from zero; the maximum significant difference is less than 5% of a cycle. The 95% confidence intervals for amplitude for the Little Skull Mountain and St. George earthquake signals suggest that the phase velocity or strain can be estimated to within about $\pm 20\%$ at frequencies between $\sim$0.04 and 0.10 Hz. Outside this band, the uncertainty estimates are generally $\sim$20 to 50%. The 95% confidence levels for the Northridge signals are $<25\%$ in only a few narrow frequency bands. To within the uncertainties, the amplitude estimates generally show a slight, and smoothly varying, offset from one for the admittance (observed/predicted). This might suggest that the phase velocity assumed was slightly in error, demonstrating that accuracy of phase velocities limits the accuracy of strain estimates from seismic data. As we will see, however, there are other possible distortions of the strain field that could also contribute to disagreements at this level (10 to 20%).

The variation in uncertainty with frequency may plausibly be attributed, in part, to the band-limited nature of seismic spectra and to the contribution of higher modes (with phase velocities that vary differently with frequency for each mode) to the seismograms. Spectra of velocity seismograms for all three earthquakes decrease below $\sim$0.05 Hz, explaining the greater uncertainties at lower frequencies. Synthetic seismogram calculations show that the most significant higher-mode energy, relative to fundamental-mode energy, exists at frequencies of $\sim$0.2 Hz and higher (Gomberg and Masters, 1988; Gomberg and Bodin, 1994; Gomberg, 1996), which may explain the generally greater uncertainties above this frequency. Furthermore, the presence of higher modes also partially explains the larger uncertainties for the Northridge earthquake relative to the other events and for the $\varepsilon_{r\phi}$

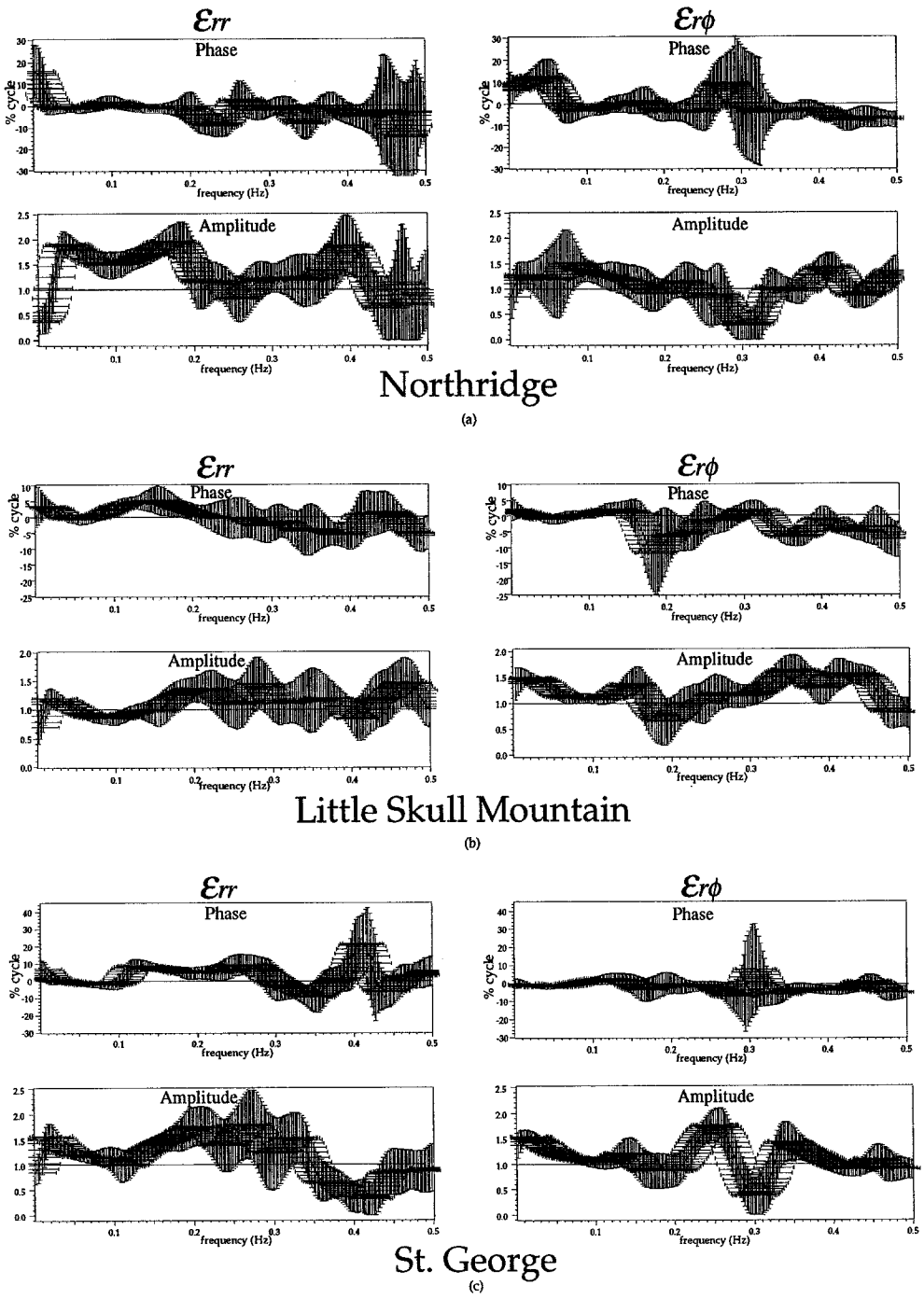

Figure 3. The phase (top) and amplitude (bottom) of Δp (equation 12) for ε_{rr}, $\varepsilon_{r\phi}$ strains calculated from seismic and strainmeter data for the same earthquake. Vertical bars indicate 95% confidence intervals, and horizontal bars equal the width of the spectral smoothing window (0.051 Hz). Phase delays corresponding to plausible clock errors, Δt, have been subtracted from each phase plot. Δts are 0.6, 0.5, and -0.1 sec for the Northridge, Little Skull Mountain, and St. George data, respectively. These errors were estimated from the trend from the phase difference calculations and by visually aligning the traces (Fig. 2). Spectral estimates are shown for data from the (a) Northridge, (b) Little Skull Mountain, and (c) St. George earthquakes.

strains relative to the ε_{rr} strains. The latter may reflect the more similar group velocities of fundamental and higher-mode Love waves relative to those for Rayleigh waves; 0.25 Hz fundamental and first higher-mode waves from the Northridge earthquake at PFO arrive in time windows separated by only ~4 sec for Love waves and ~9 sec for Rayleigh waves (according to calculations for our assumed Earth structure). These separations increase with the distance from PFO, increasing by factors of 1.7 and 2.3 for the Little Skull Mountain and St. George surface waves, respectively.

The nonzero $\varepsilon_{\phi\phi}$ strains found from the strainmeter data (Fig. 2) unambiguously indicate the presence of significant signal-associated or coherent noise, not accounted for in the cross-spectral analysis. According to Goncz and Hannan (1975), such noise can only be properly accounted for by actually modeling the process that causes it. We interpret the nonzero $\varepsilon_{\phi\phi}$ strains as indicative of our failure to model the entire process producing the observed strains; i.e., indicative of the inappropriateness of at least one of our assumptions. The rms $\varepsilon_{\phi\phi}$ strains are 0.82, 0.29, and 0.48 of the ε_{rr} strains for the Northridge, Little Skull Mountain, and St. George data, respectively; the ratio of rms $\varepsilon_{\phi\phi}$ to rms $\varepsilon_{r\phi}$ is 1.11, 0.61, and 0.62. Filtering of the data (not shown here) shows that this level of high $\varepsilon_{\phi\phi}$ strain is seen only at the higher frequencies. For the Little Skull Mountain and St. George data, low passing the data with a corner frequency of 0.1 Hz makes the $\varepsilon_{\phi\phi}$ contribution almost negligible. The processes causing this deviation from the theory must be consistent with this frequency dependence.

One possible cause of the nonzero $\varepsilon_{\phi\phi}$ strains would be epicentral errors that would cause error in the calculated receiver/source azimuth. If this were so, we should be able to find an azimuth $\tilde{\phi}$ that satisfies the equation (from equation 7):

$$\varepsilon_{\phi\phi}^{\text{local}} = \varepsilon_{xx}^{\text{global}} \cos^2 \tilde{\phi} + \varepsilon_{yy}^{\text{global}} \sin^2 \tilde{\phi} - \varepsilon_{xy}^{\text{global}} 2 \cos \tilde{\phi} \sin \tilde{\phi} = 0. \quad (13)$$

We calculated average measures of $\varepsilon_{\phi\phi}$ strains for the strainmeter data (rms and mean absolute values) for each earthquake, for $\tilde{\phi} = 0°$ to 360° at increments of 0.25°. Although there are azimuths that give minima in these average measures, these minima are only a few percent smaller than their values at the calculated azimuths. No single deviation of the propagation path can explain the result. We also tested the possibility that the apparent azimuth (propagation direction at the receiver) could be varying with time. This might arise from distortion of propagation paths (but not the wave fronts) due to material heterogeneities or topography. If true, equation (13) recast as a quadratic in tan $\tilde{\phi}$ should be solvable by allowing $\tilde{\phi}$ to vary as a function of time. However, we find that there are large time intervals during which no solution exists.

The nonzero $\varepsilon_{\phi\phi}$ strains also cannot be attributed to inappropriateness of the simplifying assumption of neglecting the curvature of cylindrical wave fronts propagating in a lateral homogeneous media. We estimated the peak curvature from the seismic data, $(u_r^{\max}/r)$, $(u_\phi^{\max}/r)$ (equation 4), for the three earthquakes. These are compared to the corresponding observed peak strains, $\varepsilon_{rr}^{\max}$, $\varepsilon_{r\phi}^{\max}$, measured by the strainmeters. The largest error of only ~3% is obtained for the closest and largest event, the Northridge earthquake.

We suggest that the nonzero $\varepsilon_{\phi\phi}$ strains reflect perturbing effects of lateral material heterogeneities and topography, combining to (1) distort the local strain field for any applied strain, static or dynamic, and (2) scatter the surface waves so that there is no single azimuth from which energy is arriving. Such effects are likely to be more severe for waves sampling shallower depths and, thus, more strongly effect higher frequencies as observed. For the first effect, Berger and Beaumont (1976) showed that a "homogenous-applied" strain field, a uniform strain input to the base of the crust below the heterogeneous region, can be locally perturbed by as much as ~17% at PFO (Fig. 4a). They derived transformation matrices, $\underline{T(x,y)}$, that describe the cross-coupling of strain components (Fig. 4b). These matrices are calculated using finite-element and prismatic-space models of the topography and possible material heterogeneities in the vicinity of PFO. At any point, the perturbed static strain field is

$$\underline{\varepsilon}^{\text{perturbed}} = \underline{T}\underline{\varepsilon}^{\text{applied}}. \quad (14)$$

Berger and Beaumont's (1976) results show that at the location of PFO, the largest off-diagonal terms of $\underline{T(x,y)}$ are ~8% and that at some locations, these cross-coupling terms may be as large as ~17%. However, the dynamic strain field is not uniformly applied to the base of the crust but instead is a laterally traveling wave. These waves may be locally distorted as they travel so that the cumulative affect may be considerably greater than 17%. The spatial variation would also predict that the distortion would vary depending on the azimuth and length of the travel path. Attributing the nonzero $\varepsilon_{\phi\phi}$ strains to this type of distortion is at least qualitatively consistent with the observation that the $\varepsilon_{\phi\phi}$ amplitudes are largest for the Northridge earthquake strains. The azimuth of the great-circle path from Northridge to PFO is closest to the trend of the greatest topographic relief, relative to the paths connecting PFO and the St. George and Little Skull Mountain epicenters.

Conclusions

We have evaluated the probable accuracy of estimates of the dynamic strain field calculated from seismic data. Cross-spectral analysis using both seismic and strain data recorded at PFO was applied to quantify uncertainties and errors that arise from random noise. Characteristics of the strainmeter data alone provided measures of the uncertainties and errors that are due to inappropriate assumptions. Cross-spectral analysis results of PFO data for the St. George

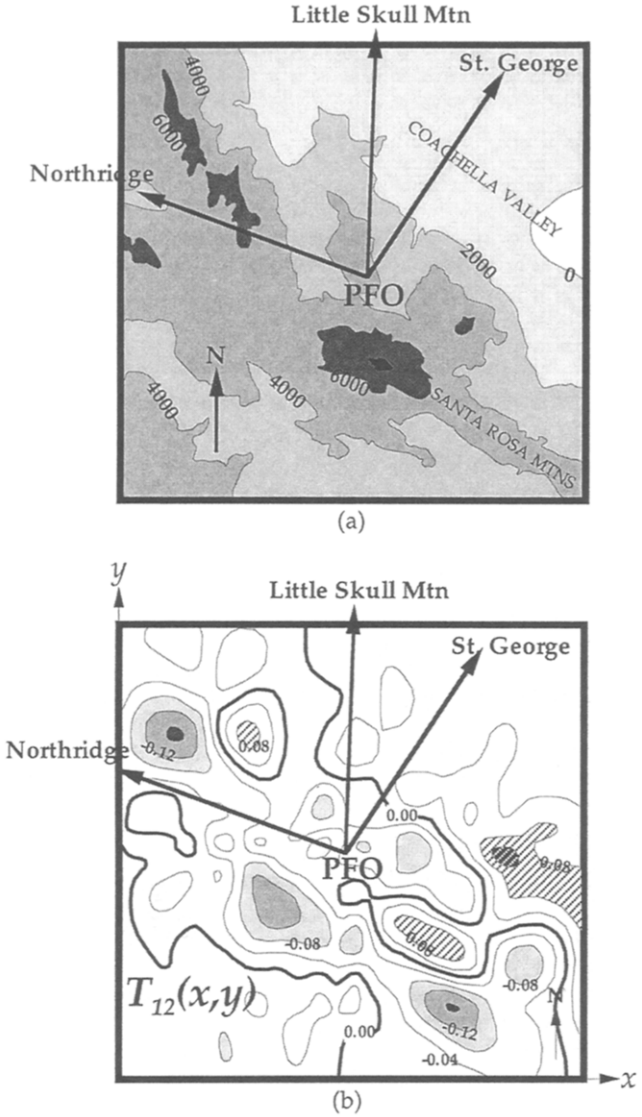

Figure 4. From Berger and Beaumont (1976). (a) 1:62500 topographic map of the PFO region. Contours are at 2000-foot intervals. Arrows indicate the azimuths to each earthquake studied. (b) Contours (at intervals of 0.04) of the T_{12} element of the transformation matrix describing the coupling of strain components. Almost all elements of the matrix show a similar pattern with the highest values and greatest variability trending northwest–southeast, closest to the Northridge-PFO propagation path.

and Little Skull Mountain earthquakes indicated that the phase characteristics of the dynamic strains can be found from the seismic data to within ±10% of a cycle (95% confidence level) below ~0.15 Hz; at higher frequencies, the uncertainties increase. Strain amplitudes are predicted with uncertainties of about ±20% at frequencies ~0.04 to 0.10 Hz and 20 to 50% at other frequencies (for our assumed Earth model). For the Northridge earthquake, "true" amplitudes are predicted with uncertainties of ±25% only in a few narrow frequency bands and are worse elsewhere. The variation in uncertainty with frequency may be attributed, in part, to the band-limited nature of seismic spectra. The contribution of higher modes to the seismograms also contributes to the frequency dependence of the uncertainties as well as to the greater uncertainties for the Northridge data.

The analysis results provide some indication of the existence of a much more significant source of uncertainty and error, that is, inappropriate assumptions about the heterogeneity of the Earth structure. The theory for the seismic strains requires the $\varepsilon_{\phi\phi}$ strains to be zero. This is not true for any of the earthquakes studied; in the worst case, the rms $\varepsilon_{\phi\phi}$ strain from the Northridge earthquake is actually larger than the rms $\varepsilon_{r\phi}$ component. We show that the nonzero $\varepsilon_{\phi\phi}$ strains cannot be attributed, to any significant degree, to (1) epicentral and azimuthal errors, (2) propagation paths deviating from great circles, or (3) approximating cylindrical wave fronts as planar. The most probable cause is local distortion of the strain field, or equivalently of the wave front, by topography and material heterogeneities and scattering of the waves by the same.

Acknowledgments

The authors thank Edward Cranswick, Scott Davis, and two anonymous reviewers for thoughtful reviews of this article and Frank Wyatt for advice on the data. Joan Gomberg's contribution was supported by a USGS Gilbert Fellowship, and Duncan Agnew's, by the USGS External Program and by the NSF. This article is CERI Contribution Number 248.

References

Agnew, D. C. (1986). Strainmeters and tiltmeters, *Rev. Geophys.* **24,** 579–624.

Anderson, J. G., J. N. Brune, J. Louie, Y. Zeng, M. Savage, G. Yu, Q. Chen, and D. dePolo (1994). Seismicity in the western Great Basin apparently triggered by the Landers, California, earthquake, 28 June 1992, *Bull. Seism. Soc. Am.* **84,** 863–891.

Ariman, T. and M. Hamada (1981). Experimental investigations on seismic behavior of buried pipelines, in *Lifeline Earthquake Engineering,* D. J. Smith (Editor), Am. Soc. Civil Eng., New York, 48–64.

Beaumont, C. and J. Berger (1975). An analysis of tidal strain observations from the United States of America I. The homogenous tide, *Bull. Seism. Soc. Am.* **65,** 1613–1629.

Benioff, H. (1935). A linear strain seismograph, *Bull. Seism. Soc. Am.* **25,** 283–309.

Benioff, H. and B. Gutenberg (1952). The response of strain and pendulum seismographs to surface waves, *Bull. Seism. Soc. Am.* **43,** 229–237.

Berger, J., D. C. Agnew, R. L. Parker, and W. E. Farrell (1979). Seismic system calibration: 2. Cross-spectral calibration using random binary signals, *Bull. Seism. Soc. Am.* **69,** 271–288.

Berger, J. and C. Beaumont (1976). An analysis of tidal strain observations from the United States of America II. The inhomogeneous tide, *Bull. Seism. Soc. Am.* **66,** 1821–1846.

Berger, J. and R. Lovberg (1970). Earth strain measurements with a laser interferometer, *Science* **170,** 296–303.

Bodin, P., R. Bilham, J. Bear, J. Gomberg, and K. Hudnut (1994). Slip triggered on southern California faults by the Landers earthquake sequence, *Bull. Seism. Soc. Am.* **84,** 806–816.

Borcherdt, R. D. (1988). Volumetric strain in relation to particle displacements for body and surface waves in a general viscoelastic halfspace, *Geophys. J. R. Astr. Soc.* **70,** 621–638.

Borcherdt, R. D., M. J. S. Johnston, and G. Glassmoyer (1989). On the use of volumetric strain meters to infer additional characteristics of short-period seismic radiation, *Bull. Seism. Soc. Am.* **79,** 1006–1023.

Cranswick, E., M. Meremonte, and A. Frankel (1994). Correlation of waveform incoherence with site amplification of Northridge aftershocks recorded by small-aperture arrays, *EOS* **75,** 168.

Der Kiureghian, A. (1994). *Proc. Fifth U.S. Natl. Conf. Earthquake Eng., Earthquake Awareness and Mitigation Across the Nation, Vol. I,* Earthquake Eng. Res. Inst., July 10–14, 1994, Chicago, Illinois, 540–550.

Dobry, R., K. H. Stokoe, R. S. Ladd, and T. L. Youd (1981). Liquefaction susceptibility from S-wave velocity, In situ testing to Evaluate Liquefaction Susceptibility, *Proc. of ASCE Natl. Convention.*

Drnevich, V. P. and F. E. Richart, Jr. (1970). Dynamic prestraining of dry sand, *J. SMFD ASCE* **96,** 453–469.

Emter, D. and W. Zurn (1985). Observations of local elastic effects on earth tide strains and tilts, in *Earth Tides,* J. C. Harrison (Editor), Van Nostrand Reinhold, New York, pp. 309–327.

Fix, J. E. (1973). Strain-inertial seismograph complexes, Rep. TR-73-16, NTIS AD-A005 708/3GI, Teledyne-Geotech, Garland, Texas.

Gomberg, J. (1996). Stress/Strain changes and triggering of seismicity by the Ms7.4 Landers, California earthquake, *J. Geophys. Res.,* in press.

Gomberg, J. and P. Bodin (1994). Triggering of the Little Skull Mountain, Nevada, Earthquake with dynamic strains, *Bull. Seism. Soc. Am.* **84,** 844–853.

Gomberg, J. and S. Davis (1996). Stress/Strain changes and triggering of seismicity at The Geysers, California, *J. Geophys. Res.,* in press.

Gomberg, J. and T. G. Masters (1988). Waveform modeling using locked-mode synthetic and differential seismograms—application to determination of the structure of Mexico, *Geophys. J. R. Astr. Soc.* **94,** 193–218.

Goncz, J. H. and E. J. Hannan (1975). New methods of estimating dispersion from stacks of surface waves, *Bull. Seism. Soc. Am.* **65,** 1519–1529.

IRIS (Incorporated Research Institutions for Seismology) (1994). Federation of Digital Seismograph Network Station Book.

Hill, D., P. Reasenberg, A. Michael, W. Arabasz, G. Beroza, D. Brumbaugh, J. Brune, R. Castro, S. Davis, D. dePolo, W. Ellsworth, J. Gomberg, S. Harmsen, L. House, S. M. Jackson, M. Johnston, L. Jones, R. Keller, S. Malone, L. Munguia, S. Nava, J. Pechmann, A. Sanford, R. Simpson, R. Smith, M. Stark, M. Stickney, A. Vidal, S. Walter, V. Wong, and J. Zollweg (1993). Seismicity remotely triggered by the Magnitude 7.3 Landers, California earthquake, 1992, *Science* **260,** 1617–1623.

Holzer, T. L., T. L. Youd, and T. C. Hanks (1989). Dynamics of liquefaction during the 1987 Superstition Hills, California, earthquake, *Science* **244,** 56–59.

Jeng V. and K. Kasai (1994). *Proc. Fifth U.S. Natl. Conf. Earthquake Eng., Earthquake Awareness and Mitigation Across the Nation, Vol. I,* Earthquake Eng. Res. Inst., July 10–14, 1994, Chicago, Illinois, 531–540.

Jenkins, G. M. and D. G. Watts (1968). *Spectral Analysis and Its Applications,* Holden-Day, San Francisco, California, chap. 8–10, 321–458.

Kanamori, H., E. Hauksson, and T. Heaton (1991). TERRAscope and CUBE project at Caltech, *EOS* **72,** 564.

Mavko, G. M. and E. Harp (1984). Analysis of wave-induced pore pressure changes recorded during the 1980 Mammoth Lakes, California, earthquake sequence, *Bull. Seism. Soc. Am.* **84,** 1395–1407.

Meremonte, M., A. Frankel, and E. Cranswick (1994). Observations of basin surface waves from Northridge aftershocks recorded by small-aperture arrays, *EOS* **75,** 168.

Mikumo, T. and K. Aki (1964). Determination of local phase velocity by intercomparison of seismograms from strain and pendulum instruments, *J. Geophys. Res.* **69,** 721–731.

Nisho, N. (1989). Dynamic strains in buried pipelines due to soil liquefaction, in *Earthquake Behavior of Buried Pipelines, Storage, Telecommunications, and Transportation Facilities,* K. Fujita, M. Hamada, M. Shinozuka, and T. Ariman (Editors), Am. Soc. Civil Eng., New York, pp. 83–88.

O'Rourke, M. J. and G. Castro (1981). Design of buried pipelines for wave propagation, in *Lifeline Earthquake Engineering,* D. J. Smith (Editor), Am. Soc. Civil Eng., New York, pp. 32–47.

Romney, C. (1964). Combinations of strain and pendulum seismographs for increasing the detectability of P, *Bull. Seism. Soc. Am.* **54,** 2165–2174.

Sacks, S., J. A. Snoke, R. Evans, G. King, and J. Beavan (1976). Single-site phase velocity measurements, *Geophys. J. R. Astr. Soc.* **46,** 253–258.

Seed, H. B. and I. M. Idriss (1971). A simplified procedure for evaluating soil liquefaction potential, *Am. Soc. Civil Eng. Proc.* **97,** 1249–1274.

Spudich, P., D. Harlow, W. H. K. Lee, J. Rogers, and R. White (1994). Strong site effects observed at the Tarzana accelerograph site using aftershocks of the 1994 Northridge, California, earthquake: implications for seismic microzonation (Abstract), *Seism. Soc. Am. Meeting,* Pasadena.

Spudich, P., L. K. Steck, M. Hellweg, J. B. Fletcher, and L. Baker (1995). Transient stresses at Parkfield, California, produced by the M 7.4 Landers earthquake of June 28, 1992: observations from the Upsar dense seismograph array. *J. Geophys. Res.* **100,** 675–690.

Stewart, H. E. and A. K. Hussein (1992). Determination of the dynamic shear modulus of Holocene bay mud for site-response analysis, in The Loma Prieta, California, Earthquake of October 17, 1989—Marina District, *U.S. Geol. Surv. Profess. Paper 1551-F,* T. D. O'Rourke (Editor), 75–84.

Wang, J. and T. Teng (1994). Surface wave profiling of the lithosphere beneath the Mojave desert using TERRAscope data, *J. Geophys. Res.* **99,** 743–750.

Woodhouse, J. H. (1974). Surface waves in a laterally, varying structure, *Geophys. J. R. Astr. Soc.* **37,** 461–490.

Wyatt, F. K. (1988). Measurements of coseismic deformation in southern California: 1972–1982, *J. R. Astr. Soc.* **93,** 2923–2942.

Zerva, A. (1992a). Spatial incoherence effects on seismic ground strains, *Probabilistic Eng. Mech.* **7,** 217–226.

Zerva, A. (1992b). Seismic loads predicted by spatial variability models, *Structural Safety* **11,** 227–243.

U.S. Geological Survey
CERI, University of Memphis
Memphis, Tennessee 38152
(J.G.)

IGPP A-025
University of California, San Diego
La Jolla, California 92093-0225
(D.A.)

Manuscript received 10 January 1995.